Journal of Power Sources 217 (2012) 498–502

Contents lists available at SciVerse ScienceDirect

Journal of Power Sources

journal homepage: www.elsevier.com/locate/jpowsour

Short communication

Enhanced electrocatalytic oxidation of urea based on nickel hydroxide nanoribbons

Dan Wang, Wei Yan, Santosh H. Vijapur, Gerardine G. Botte*

Center for Electrochemical Engineering Research, Chemical and Biomolecular Engineering Department, 165 Stocker Center, Ohio University, Athens, OH 45701, USA

HIGHLIGHTS

► One-dimensional nickel hydroxide nanoribbons were synthesized through a simple template-free hydrothermal method.
► The nickel hydroxide nanoribbons were developed as efficient electrocatalysts for urea electrocatalytic oxidation.
► More than 10 times enhancement in current density compared to bulk nickel hydroxide powders.

ARTICLE INFO

Article history:
Received 2 April 2012
Received in revised form
4 June 2012
Accepted 6 June 2012
Available online 13 June 2012

Keywords:
Nickel hydroxide nanoribbons
Urea oxidation
Electrocatalysts
Hydrogen production
Fuel cells

ABSTRACT

One-dimensional nickel hydroxide nanoribbons with thickness of 15–20 nm and length up to several micrometers were synthesized through a simple template-free hydrothermal method. The nickel hydroxide nanoribbons were developed as electrocatalysts for urea electro-oxidation in alkaline media and showed more than 10 times enhancement in current density compared to bulk nickel hydroxide powders. The enhanced electrocatalytic oxidation of urea using nickel hydroxide nanoribbons reveals great potential for future applications in hydrogen production, remediation of urea-rich wastewater, and fuel cells.

1. Introduction

One-dimensional (1 D) nanostructures with large surface areas and quantum confinement effect have attracted increasing interests in both fundamental research and technological applications over the past two decades. Due to their excellent electrical, mechanical, optical and chemical properties, 1 D nanomaterials, such as nanotubes, nanowires, nanorods, and nanobelts/nanoribbons, have been widely used as electrode materials in solar cells, batteries, supercapacitors, fuel cells and sensors [1–5]. Nickel hydroxide is a well-known positive electrode material in a number of Ni-based alkaline rechargeable batteries, such as Ni–MH, Ni–Cd, and Ni–Zn batteries, due to its well-defined redox behavior, low cost, and high power density [6–8]. Nickel hydroxides with one-dimensional structures can be synthesized through different methods, such as electroless deposition [9], hydrothermal synthesis [10–12], and template-directed synthesis [13,14]. The nanostructured nickel hydroxide has shown increasing discharge capacities in Ni–MH batteries [11,14].

As an animal feed additive and nitrogen-release fertilizer, urea is extremely important for the agricultural industry. Moreover, urea has been demonstrated as a hydrogen carrier for long-term sustainable energy supply [15,16]. However, urea-rich wastewater is also produced during the industrial synthesis of urea. Effective methods for urea removal/decomposition during wastewater treatment are therefore necessary for both environmental and energy reasons. The biocatalytic decomposition of urea has been extensively investigated in the past [17–20]. This enzyme catalyzed reaction releases large amounts of toxic ammonia. Ammonia emissions to the atmosphere can impair air quality. In addition, the immobilization, denaturation, and deactivation of the urease enzyme will also limit the long term and large-scale decomposition of urea.

Electrocatalytic oxidation with noble metal catalysts was introduced as an approach for urea decomposition, which avoids the use of urease enzyme and the production of toxic ammonia

* Corresponding author. Tel.: +1 740 593 9670; fax: +1 740 593 0873.
E-mail address: botte@ohio.edu (G.G. Botte).

0378-7753/$ – see front matter © 2012 Elsevier B.V. All rights reserved.
http://dx.doi.org/10.1016/j.jpowsour.2012.06.029

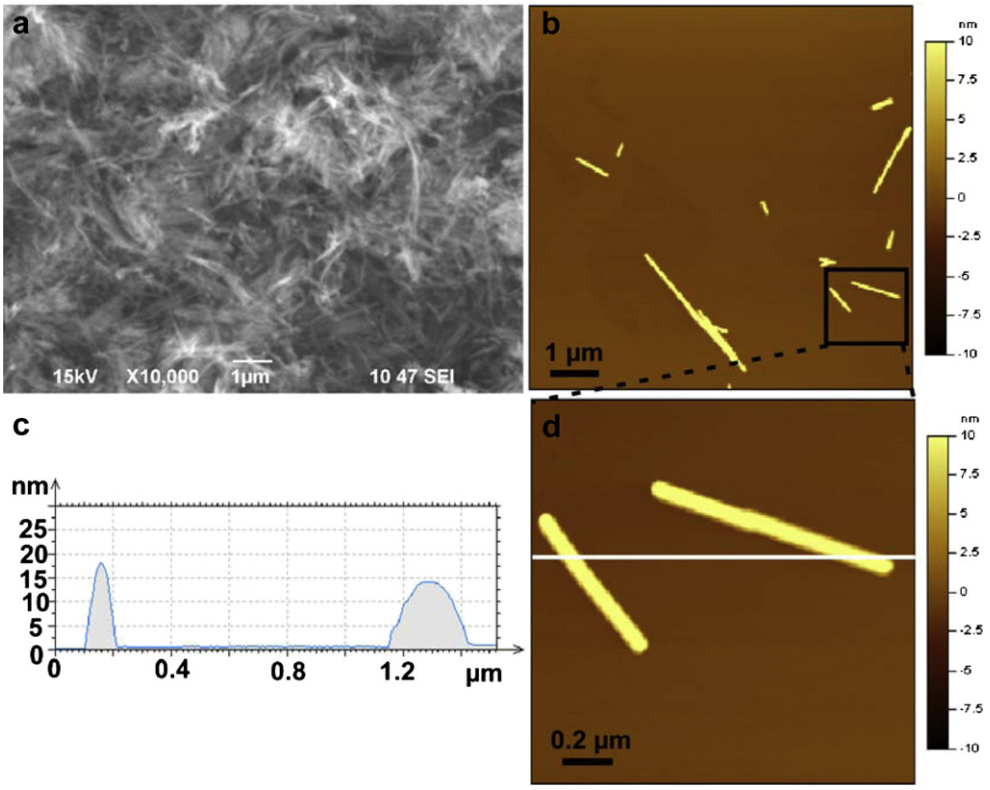

Fig. 1. Electron microscope images of nickel hydroxide nanoribbons. (a) SEM and (b) AFM images of nickel hydroxide nanoribbons. (c) Height profile of nickel hydroxide nanoribbons in AFM image (d). (d) AFM image of the part surrounded by the black frame in (b).

[21]. Recently, nickel hydroxide was developed as a catalyst for urea electrolysis that directly converts urea to benign nitrogen and to clean fuel hydrogen [16,22], according to the following reactions:

$$CO(NH_2)_{2(aq)} + 6OH^- \rightarrow N_{2(g)} + 5H_2O_{(1)} + CO_{2(g)} + 6e^- \quad (1)$$

$$6H_2O_{(1)} + 6e^- \rightarrow 3H_{2(g)} + 6OH^-_{(aq)} \quad (2)$$

Reaction (1) takes place at the anodic compartment of the urea electrolyzer, while reaction (2) takes place at the cathodic compartment of the cell. The overall reaction is given by

$$CO(NH_2)_{2(aq)} + H_2O_{(1)} \rightarrow N_{2(g)} + 3H_{2(g)} + CO_{2(g)} \quad (3)$$

Hydrogen gas can be produced on demand in the process at a standard theoretical cell voltage of 0.37 V.

The development of bulk nickel hydroxides as catalysts for urea electrolysis not only alleviated the requirement for expensive noble metal catalysts, but also improved the urea oxidation rate considerably during the electrocatalytic oxidation process [16,23–25]. Exfoliated nickel hydroxide nanosheets enhanced the urea electrolysis [26], although the yield and synthesis process of the nanosheets need to be promoted. Since the properties and applications of 1 D nanostructures are superior to their bulk counterparts due to their large surface areas and quantum confinement effect [1], it is thus intriguing to extend the applications of one-dimensional nickel hydroxide nanoribbons to urea electrolysis for hydrogen production. Within this context, the authors synthesized one-dimensional nickel hydroxide nanoribbons through a simple template-free hydrothermal method and developed the 1D nanoribbons as electrocatalysts for urea electrocatalytic oxidation.

2. Materials and methods

2.1. Chemicals

Nickel (II) sulfate heptahydrate (Ni 20–21%) and ethanol (HPLC grade) were purchased from Acros Organics. Potassium hydroxide pellets (85.0+%), ammonium hydroxide (29.5%), and urea (99.7%) were obtained from Fisher Scientific. Polytetrafluoroethylene (PTFE) (60 wt.%) was received from Sigma-Aldrich. Commercial bulk nickel (II) hydroxide powder (Ni 61%) was purchased from Alfa Aeaser.

2.2. Nickel hydroxide nanoribbon synthesis

The nickel hydroxide nanoribbons were synthesized through hydrothermal treatment [10–12]. In a typical experiment, 5 mmol of nickel (II) sulfate heptahydrate was dissolved in 24 ml of deionized water to form a green $NiSO_4$ solution, then 6 ml of 1 M ammonium hydroxide was added into the $NiSO_4$ solution with stirring. The mixed solution was heated at 180 °C for 24 h in a sealed Teflon-lined autoclave, then cooled down to room temperature. The green precipitate was collected by centrifugation at 4000 rpm for 10 min, washed with deionized water for three times by shaking and centrifugation, and finally dried at 40 °C in an oven overnight.

2.3. Characterization

The morphologies and sizes of the synthesized nickel hydroxide nanoribbons were characterized by scanning electron microscopy (SEM, JEOL-JSM-6390LV) and atomic force microscopy (AFM, Agilent Technologies 5500). The AFM images were taken at room

temperature and under ambient conditions in AC mode with NSC15/AlBS probes from MikroMasch USA (Wilsonville, OR). The surface area of the nickel hydroxide nanoribbons was measured by the Brunauer–Emmer–Teller (BET)method using a TriStar II 3020 surface area analyzer (Micromeritics). The nickel hydroxide nanoribbons were degasified overnight at 80 °C using nitrogen gas prior to the BET measurements. Powder X-ray diffraction (XRD) analysis were obtained on a Rigaku Ultima IV X-Ray Diffractometer with monochromatic Cu Kα radiation ($\lambda = 0.15405$ nm) at a scanning rate of 2 ° min^{-1}. The Raman spectra were recorded using Bruker Senterra Raman spectrometer and microscope through a 10X objective lens using a 100 mW 532 nm laser excitation. Fourier transform infrared (FTIR) spectra were measured by transmission on a Bruker Vertex 80 FT-IR Spectrometer on KBr pellets with 2 cm^{-1} resolution.

2.4. Electrode preparation and electrochemical measurements

Glassy carbon electrodes (GCE, 3.0 mm diameter) were purchased from CH Instruments, Inc. GCEs were first polished with 1 μm polishing alumina, and rinsed with deionized water. The electrodes were further polished with 0.05 μm polishing alumina, rinsed with deionized water, and then sonicated in deionized water for 10 minutes to remove alumina particles, finally dried with a flow of Argon (99.999% purity) and used as substrates for nickel hydroxide nanoribbon modification.

Nickel hydroxide nanoribbons were sonicated in ethanol for 10 min to get nanoribbon suspensions with the concentration of 10 mg ml^{-1}. 2 μl of nickel hydroxide nanoribbon suspension was dropped on polished GCE and dried at 50 °C. 2 μl of 60% PTFE solution was dropped on the nanoribbon GCE and allowed for drying at 50 °C about 3 min, the electrode was then pressed against a weighting paper for abrasively attaching nickel hydroxide nanoribbon to GCE surface and dried at 50 °C overnight. After drying, the nanoribbon modified electrode was activated by 50 cycles of cyclic voltammetries from 0 to 0.65 V vs. Hg/HgO at 20 mV s^{-1} in 5 M KOH and then used as working electrode in all electrochemical measurements. The control experiments used the bulk nickel hydroxide powder with the PTFE binder modified GCE as the working electrode.

All electrochemical measurements were performed in 5 M KOH solution in the absence and presence of 0.33 M urea using a Solartron 1470E potentiostat. Hg/HgO electrode and platinum foil (2 cm × 1 cm) were chosen as the reference and counter electrodes, respectively. The cyclic voltammograms (CVs) were obtained between 0 V to 0.65 V vs. Hg/HgO at a scan rate of 10 mV s^{-1}. All the voltammograms reported are the sustained periodic state achieved after 20 sweeps. The chronoamperograms were carried out at a constant potential of 0.50 V vs. Hg/HgO for 1 h.

3. Results and discussion

3.1. Characterization of nickel hydroxide nanoribbons

The morphology and size of the nickel hydroxide nanoribbon samples were characterized by SEM and AFM images. The SEM image (Fig. 1a) shows a large quantity of ribbon like nanostructures with the length up to several micrometers in the obtained samples. Consistent with SEM observations, the samples were further investigated using AFM. In order to take AFM images, the ribbon like nickel hydroxide products were first dispersed in ethanol by 10 min of sonication, followed by 10 min of centrifugation at 4000 rpm. 10 μl of the resulting suspension was then directly dropped on to a piece of freshly cleaved mica for AFM measurements. The AFM images (Fig. 1b and d) indicate the samples have ribbon like structures and the corresponding height measurement (Fig. 1c) shows the samples have typical thickness of about 15–20 nm. The BET specific surface area of nickel hydroxide nanoribbons was found to be 54.9 $m^2 g^{-1}$. As a comparison, bulk nickel hydroxide powders exhibited a BET surface area of 5.8 $m^2 g^{-1}$.

The structures and composition of the obtained nickel hydroxide nanoribbons were studied by XRD, Raman spectroscopy, and FTIR spectroscopy. Fig. 2a shows the XRD pattern of

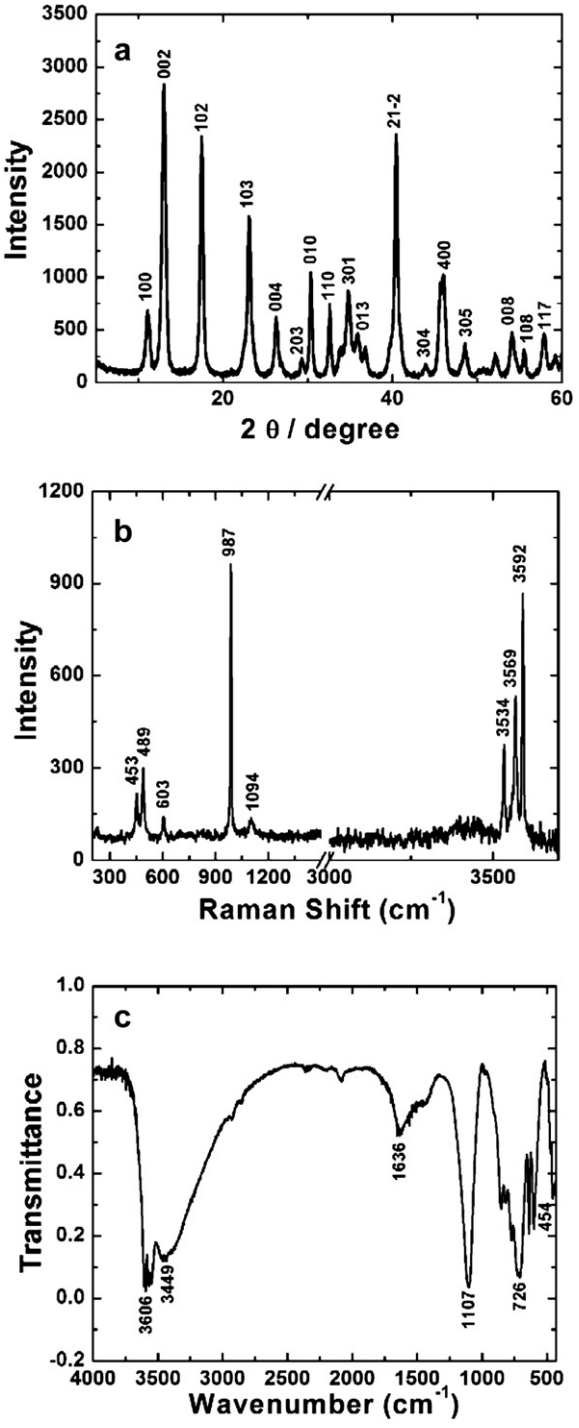

Fig. 2. Structure and composition characterization of nickel hydroxide nanoribbons. (a) XRD pattern, (b) Raman spectrum, and (c) FTIR spectrum of nickel hydroxide nanoribbons.

synthesized nickel hydroxide nanoribbons. All the diffraction peaks can be indexed to the monoclinic phase nickel hydroxide and are well consistent with the standard card JCPDS No.41-1424. The Raman spectrum of the nickel hydroxide nanoribbons is shown in Fig. 2b. The peaks at 453 and 489 cm^{-1} can be assigned to the Ni–OH stretching mode and the Ni–O vibration, respectively [27]. The peaks at 603, 987, and 1094 cm^{-1} are due to the adsorbed sulfate anions, which indicates that the nickel hydroxide nanoribbons contain the intercalated sulfate anions [28]. The peaks around 3600 cm^{-1} result from the stretching vibrations of the hydroxide groups of nickel hydroxide and hydrogen bonded hydroxide groups due to the adsorbed water [11,28]. The structural information of nickel hydroxide nanoribbons was further confirmed by FTIR spectrum. As shown in Fig. 2c, the peak at 454 cm^{-1} can be assigned to the Ni–OH stretching mode and the complex system of peaks in the range of 600–1200 cm^{-1} are attributed to the intercalated sulfate species [28,29]. The broad bands at 1636 and 3349 cm^{-1} are due to the bending and stretching vibrations of the adsorbed water and the band around 3600 cm^{-1} is attributed to O–H stretching vibrations [29,30].

3.2. Electrocatalytic oxidation of urea based on nickel hydroxide nanoribbons

The electrochemical behavior of the nickel hydroxide nanoribbon modified electrodes was first investigated by cyclic voltammetry (CV). The CV of nickel hydroxide nanoribbon modified electrodes in 5 M KOH is shown in Fig. 3a (curve 1). The anodic peak is due to the oxidation reaction of Ni^{2+} to Ni^{3+}, and the cathodic peak is for the reverse process. A strong oxidation current starting at ca. 0.45 V and a peak current at ca. 0.50 V vs. Hg/HgO are shown in the curve 2 (Fig. 3a), when 0.33 M urea was present in the KOH solution. The drastic increase of oxidation current is due to the urea electro-oxidation catalyzed by $Ni(OH)_2$/NiOOH redox couple in alkaline media [16,24,25,31].

Chronoamperograms were used to further evaluate the electrocatalytic activities of nickel hydroxide nanoribbons for urea electrolysis. A constant voltage (0.50 V vs. Hg/HgO) was chosen as the applied potential according to the oxidation peak potential of urea (Fig. 3a curve 2). The chronoamperograms show a continuous, constant, and higher current density (Fig. 3b curve 2) when urea was present in the KOH solution, which indicates that nickel hydroxide nanoribbons are stable and active electrocatalysts for urea oxidation in alkaline media. Due to the consumption of urea from the electrolyte, the oxidation current slightly decreases with time (Fig. 3b curve 2).

As a comparison, the electro-oxidation of urea was studied using bulk nickel hydroxide powder modified electrodes. Both CVs (Fig. 3c) and chronoamperograms (Fig. 3d) show that bulk nickel hydroxide can also catalyze urea electrolysis. However, the urea oxidation current catalyzed by nickel hydroxide nanoribbons is more than 10 times higher than that of bulk nickel hydroxide powders. It has been reported that high surface area forms of the nickel hydroxide can markedly enhance the oxidation current densities of small organic compounds [32]. The electroactive surface area (ESA) of the nickel hydroxide nanoribbons and the bulk nickel hydroxide powders was estimated according to the following equation [33–35]:

$$\mathrm{ESA} = Q/(mq)$$

Where Q is the charge required to reduce NiOOH to $Ni(OH)_2$, which can be calculated from the cyclic voltammograms (curve 1 in Fig. 3a and c), m is the loading amount of the nickel catalysts, and q is the charge associated with the formation of a monolayer of $Ni(OH)_2$. Since the formation of $Ni(OH)_2$ from NiOOH involves one electron, the q can be taken as 257 μC cm^{-2} [36–38]. The electroactive surface

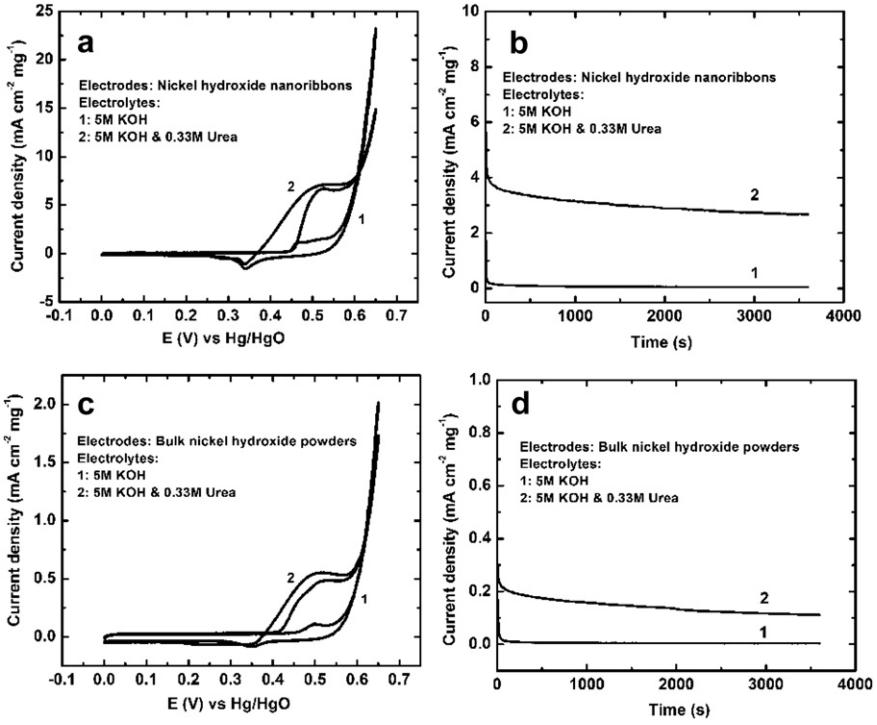

Fig. 3. Electrochemical analysis of nickel hydroxide nanoribbon modified electrodes for urea electrocatalytic oxidation. CVs of nickel hydroxide nanoribbon (a) and bulk nickel hydroxide powder (c) modified GCEs in 5 M KOH solution in the absence (curve 1) and presence (curve 2) of 0.33 M urea. The scan rate was 10 mV s^{-1}. Chronoamperograms of nickel hydroxide nanoribbon (b) and bulk nickel hydroxide powder (d) modified GCEs in 5 M KOH solution in the absence (curve 1) and presence (curve 2) of 0.33 M urea. The applied potential was 0.5 V vs. Hg/HgO.

areas of nickel hydroxide nanoribbons and bulk nickel hydroxide powders were then calculated to be 2114 $cm^2 g^{-1}$ and 97 $cm^2 g^{-1}$, respectively. The large surface area of 1 D nickel hydroxide nanoribbons promotes electron transfer of urea oxidation and enhances the current density during the urea oxidation process.

4. Conclusions

One-dimensional nickel hydroxide nanoribbons were synthesized through a simple template-free hydrothermal method and used as electrocatalysts for the electrocatalytic oxidation of urea. SEM, AFM, BET, XRD, Raman spectroscopy, FTIR spectroscopy, cyclic voltammetry, and chronoamperometry techniques were used to characterize the nickel hydroxide nanoribbons. The electrochemical analysis showed that the urea oxidation current due to the nickel hydroxide nanoribbons is more than 10 times higher than that of the bulk nickel hydroxide powders. The enhanced electrocatalytic oxidation of urea using nickel hydroxide nanoribbons reveals great potential for future applications in hydrogen production, urea-rich wastewater remediation, and fuel cells. The increase in the current density obtained represents a significant progress towards building compact urea electrolyzers for the production of hydrogen on demand.

Acknowledgments

The authors would like to thank the financial support of the Center for Electrochemical Engineering Research at Ohio University, and the Department of Defense through the U.S. Army Construction Engineering Research Laboratory (W9132T-09-1-0001). The content of the information does not reflect the position or the policy of the U.S. government.

References

[1] Y. Xia, P. Yang, Y. Sun, Y. Wu, B. Mayers, B. Gates, Y. Yin, F. Kim, H. Yan, Adv. Mater. 15 (2003) 353–389.
[2] N.-S. Choi, Y. Yao, Y. Cui, J. Cho, J. Mater. Chem. 21 (2011) 9825–9840.
[3] Q. Zhang, G. Cao, Nano Today 6 (2011) 91–109.
[4] K. Balasubramanian, Biosens. Bioelectron. 26 (2010) 1195–1204.
[5] R. Liu, J. Duay, S.B. Lee, Chem. Commun. 47 (2011) 1384–1404.
[6] J. Chen, F. Cheng, Acc. Chem. Res. 42 (2009) 713–723.
[7] W.-K. Hu, D. Noreus, Chem. Mater 15 (2003) 974–978.
[8] L.J. Yang, X.P. Gao, Q.D. Wu, H.Y. Zhu, G.L. Pan, J. Phys. Chem. C 111 (2007) 4614–4619.
[9] M. Kawamori, S. Yagi, E.-I. Matsubara, J. Electrochem. Soc. 158 (2011) E79–E83.
[10] L. Dong, Y. Chu, W. Sun, Chem.–Eur. J. 14 (2008) 5064–5072.
[11] D. Yang, R. Wang, M. He, J. Zhang, Z. Liu, J. Phys. Chem. B 109 (2005) 7654–7658.
[12] H. Liang, L. Liu, Z. Yang, Y. Yang, Cryst. Res. Technol. 45 (2010) 661–666.
[13] F.-S. Cai, G.-Y. Zhang, J. Chen, X.-L. Gou, H.-K. Liu, S.-X. Dou, Angew. Chem., Int. Ed. 43 (2004) 4212–4216.
[14] Y.-x. Wang, Z.-a. Hu, H.-y. Wu, Mater. Chem. Phys. 126 (2011) 580–583.
[15] A.N. Rollinson, J. Jones, V. Dupont, M.V. Twigg, Energy Environ. Sci. 4 (2011) 1216–1224.
[16] B.K. Boggs, R.L. King, G.G. Botte, Chem. Commun. (2009) 4859–4861.
[17] N.E. Dixon, C. Gazzola, R.L. Blakeley, B. Zerner, J. Am. Chem. Soc. 97 (1975) 4131–4133.
[18] W.H.R. Shaw, D.G. Walker, J. Am. Chem. Soc. 80 (1958) 5337–5342.
[19] D. Suarez, N. Diaz, K.M. Merz Jr., J. Am. Chem. Soc. 125 (2003) 15324–15337.
[20] G. Estiu, K.M. Merz Jr., J. Phys. Chem. B 111 (2007) 10263–10274.
[21] S.J. Yao, S.K. Wolfson Jr., B.K. Ahn, C.C. Liu, Nature 241 (1973) 471–472.
[22] G.G. Botte, (2009) Patent No. US 20090095636.
[23] R.L. King, G.G. Botte, J. Power Sources 196 (2011) 2773–2778.
[24] D.A. Daramola, D. Singh, G.G. Botte, J. Phys. Chem. A 114 (2010) 11513–11521.
[25] R.L. King, G.G. Botte, J. Power Sources 196 (2011) 9579–9584.
[26] D. Wang, W. Yan, G.G. Botte, Electrochem. Commun. 13 (2011) 1135–1138.
[27] Y.L. Lo, B.J. Hwang, Langmuir 14 (1998) 944–950.
[28] S. Deabate, F. Fourgeot, F. Henn, J. Power Sources 87 (2000) 125–136.
[29] D. Sun, J. Zhang, H. Ren, Z. Cui, D. Sun, J. Phys. Chem. C 114 (2010) 12110–12116.
[30] Y. Khan, S.K. Durrani, M. Mehmood, A. Jan, M.A. Abbasi, Mater. Chem. Phys. 130 (2011) 1169–1174.
[31] W. Yan, D. Wang, G.G. Botte, Electrochim. Acta 61 (2012) 25–30.
[32] K. Manandhar, D. Pletcher, J. Appl. Electrochem. 9 (1979) 707–713.
[33] B.Y. Xia, J.N. Wang, X.X. Wang, J. Phys. Chem. C 113 (2009) 18115–18120.
[34] E. Antolini, L. Giorgi, A. Pozio, E. Passalacqua, J. Power Sources 77 (1999) 136–142.
[35] E.P. Lee, Z. Peng, D.M. Cate, H. Yang, C.T. Campbell, Y. Xia, J. Am. Chem. Soc. 129 (2007) 10634–10635.
[36] S.A.S. Machado, L.A. Avaca, Electrochim. Acta 39 (1994) 1385–1391.
[37] I.J. Brown, S. Sotiropoulos, J. Appl. Electrochem. 30 (2000) 107–111.
[38] F. Hahn, B. Beden, M.J. Croissant, C. Lamy, Electrochim. Acta 31 (1986) 335–342.